Nuclear Instruments and Methods in Physics Research B 329 (2014) 40–47

Contents lists available at ScienceDirect

Nuclear Instruments and Methods in Physics Research B

journal homepage: www.elsevier.com/locate/nimb

Synthesis characterization and luminescence studies of 100 MeV Si^{8+} ion irradiated sol gel derived nanocrystalline Y_2O_3

B.N. Lakshminarasappa [a,*], N.J. Shivaramu [a], K.R. Nagabhushana [b], Fouran Singh [c]

[a] Department of Physics, Jnanabharathi Campus, Bangalore University, Bangalore 560 056, India
[b] Department of Physics (S & H), PES Institute of Technology, 100 Feet Ring Road, Banashankari 3rd Stage, Bangalore 560085, India
[c] Inter University Accelerator Centre, P.O. Box No. 10502, New Delhi 110 067, India

ARTICLE INFO

Article history:
Received 27 October 2013
Received in revised form 24 February 2014
Accepted 24 February 2014
Available online 3 April 2014

Keywords:
Y_2O_3 nanoparticals
Sol–gel synthesis
Swift heavy ions
Photoluminescence
Thermoluminescence

ABSTRACT

Nanoparticles of pure yttrium oxide (Y_2O_3) have been prepared by sol gel method. The powder X-ray diffraction (PXRD) pattern of as synthesized sample showed the amorphous nature. The as synthesized Y_2O_3 powders are annealed at 500, 600, 700, 800 and 900 °C for 2 h. Y_2O_3 powder heat treated for 600 °C showed cubic phase and the crystallite sizes are found to be ~13 nm. Fourier transformed infrared spectroscopy (FTIR) revealed absorption with peaks at 3434, 1724, 1525, 1400, 847, 562 and 465 cm^{-1}. Photoluminescence (PL) of 100 MeV Si^{8+} ion irradiated samples shows emission with peaks at 417, 432, 465 nm. It is found that PL intensity increases with increasing in ion fluence up to $\sim 3 \times 10^{12}$ ions cm^{-2} and then decreases with further increase in ion fluence. A well resolved thermoluminescence (TL) glow with peak at ~430 K (Tm_1) and an unresolved TL glow with peak at ~538 (Tm_2), 584 K (Tm_3) are observed in ion irradiated samples.

1. Introduction

Yttrium oxide is a rare earth sesquioxide which has been widely used in coating materials and as a red-emitting phosphor [1]. Y_2O_3 has cubic bixbyite type structure [2,3] and depicts two types of crystallographic sites are possible in Y_2O_3 [4]. Oxygen are located at the corner of the cube, it can be seen that with the occurrence of two oxygen vacancies along body and face diagonals leads to S6 and C2 symmetries for Y^{3+} ion. It is expected that the transparent Y_2O_3 can be used for high intensity discharge lamps, heat resistant windows and laser materials [2]. The Y_2O_3 possesses high refractory properties with melting point of ~2450 °C and thermal conductivity of 33 Wm^{-1} K^{-1}. It is a suitable material for photonic waveguide due to its high band gap (5.72 eV), with a very high refractive index (~2) and a wide transmission range (280–8000 nm). Y_2O_3 nanoparticals with strong red luminescence (quantum yield about 25%) was synthesized via simple hydroxylation of yttrium nitrate using hexamethylenetetramine as an additive; the red luminescence is emitted from oxygen-related defects of pure Y_2O_3 nanoparticals and is tunable by altering the additive [5]. Y_2O_3 nanopowder was synthesized by solution combustion technique in which EDTA-Na_2 is used as the chelating fuel. Further, the TL behavior of the γ-irradiated Y_2O_3 has been studied [6]. Various techniques are available for the preparation of nanomaterials. They include breaking down a bulk solid or building up processes. Some of the well known methods are: Chemical vapor deposition, laser abrasion, plasma synthesis, high energy milling, hydrothermal, sol–gel, spray pyrolysis method and co-precipitation method [7]. Among these techniques sol–gel process is also known as chemical solution deposition, a wet-chemical technique widely used in the fields of ceramic engineering and materials science. In sol–gel synthesis a soluble precursor molecule is hydrolyzed to form a dispersion of colloidal particles (the sol). Further reaction causes bonds to form between the sol particles resulting in an infinite network of particles (the gel). The gel is then typically heated to yield the desired material. This method is useful for the synthesis of inorganic materials at low temperature. In addition, homogeneous multi-component systems, monodisperse tubules and fibrils of the desired material are obtained. The sol–gel approach is a cheap and low-temperature technique that allows for the fine control of the product's chemical composition, large surface area and high homogeneity products. Sol–gel derived materials have diverse applications in optics, energy, space, electronics, bio sensors, medicine (e.g. controlled drug release), reactive material and chromatography [8].

Interest in ion beam irradiation of inorganic insulator has increased in recent years, prompted by the ion induced improvements of the optical properties of various inorganic insulators. A wide variety of material modification in metal oxides has been

* Corresponding author. Tel.: +91 9448116281; fax: +91 80 23219295.
E-mail address: bnlnarassappa@rediffmail.com (B.N. Lakshminarasappa).

http://dx.doi.org/10.1016/j.nimb.2014.02.128
0168-583X/

studied by using ion irradiation technique. Extensive research has focused onto swift heavy ions probably because of the large penetration length in metal oxide. It causes electronic energy loss and becomes dominant over nuclear energy loss and causes significant changes in structural and optical properties of materials and it creates defect centers [9]. Thermoluminescence (TL) is the light emission mainly in visible region that take place during heating of a sample following an earlier exposed to ionizing radiations. Material such as LiF, $CaSO_4$, CaF_2 and Al_2O_3 are good thermoluminescence phosphors because of their applications in dosimetry, age determination and geology or solid-state defect structure analysis [10]. The effective atomic number (Z_{eff}) is a fundamental property of the TL materials and it is related with radiation interaction processes and latter has direct applications in characterization of wide range of radiological dosimetry, surrogate materials, biological tissues and the calculation of particle interactions. For practical applications, such as high sensitivity of TL material must have high Z_{eff} atomic numbers. Z_{eff} of Y_2O_3 compound is 36.13 [11]. Photoluminescence (PL) is the process, in which the excitation is accomplished by the absorption of photons. The radiation source may be infrared, visible, ultraviolet or X-ray. PL is an extremely useful tool for obtaining information about the electronic, optical and photoelectric properties of materials [12].

In the present work, Y_2O_3 nanopowder is synthesized by the sol–gel technique using citric acid as chelating agent. We are reporting the effect of annealing temperatures on structure using PXRD and FTIR methods. Also experimental results of XRD, FTIR, PL and TL obtained after 100 MeV swift Si^{8+} irradiation in sol–gel synthesized nanocrystalline yttria are discussed.

2. Experimental

Nanosize yttria are synthesized by the sol gel technique using yttrium(III) nitrate hexahydrate ($Y(NO_3)_3{\cdot}6H_2O$) with the purity of 99.8% (Aldrich chemicals), citric acid anhydrous GR ($C_6H_8O_7$) with the purity of 99.5% and 25% GR ammonia solution (NH_3) (Merck specialties private limited). The ratio of citric acid/Y^{3+} consider to be 2 [13]. Stoichiometric amount of yttrium nitrate is dissolved in double distilled water and then the solution is refluxed at room temperature for 3 h and then slowly added citric acid which acts as a chelating agent and again refluxed at 75–80 °C for 1 h and then adjusted the pH to 2 by adding 25% aqueous ammonia solution. The obtained solution is refluxed at same condition for 6 h. During refluxing, the solution slowly evaporated and turned into a radish brown gel. The gel is dried at 110 °C to overnight in air and the obtained gel powder is grounded in an agate mortar and finally annealed at different temperature at 500, 600, 700, 800 and 900 °C for 2 h, in air and slowly cooled to room temperature [14]. Fig. 1 shows the flow chart for the synthesis of Y_2O_3 powder by sol–gel technique. For swift heavy ion irradiation studies, the samples annealed at 700 °C are choosen. The pellets of approximately 1 mm thickness and 5 mm diameter are prepared by applying a pressure of $\sim 4.0 \times 10^6$ Pa using an homemade pelletizer by taking ~40 mg of the sample mixing together with 4% of polyvinyl chloride solution and agate mortar [15]. These pellets are annealed at 900 °C for 2 h in air atmosphere in a muffle furnace to remove the deformations.

2.1. Characterization

The prepared yttria is characterized by X-ray diffraction (XRD) [The advanced D-8 X-ray diffractometer (Bruker AXS Germany)] using 1.5406 Å from CuKα radiations. The morphology of the synthesized sample is studied by scanning electron microscopy (JEOL JSM-840A). The Fourier transformed infrared transmittance spectra

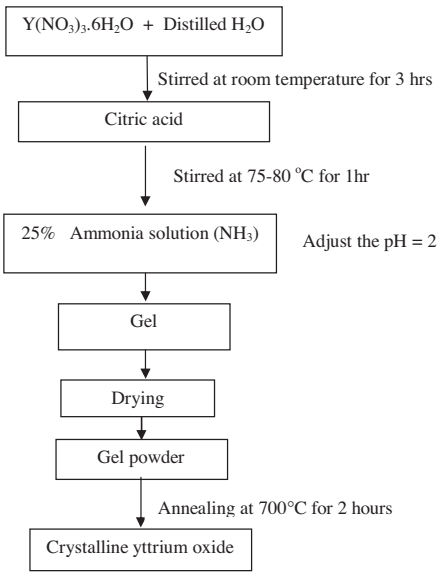

Fig. 1. Schematic flow chart for the synthesis of Y_2O_3 by sol–gel technique.

are recorded using Nicollet Magna 550 spectrophotometer. One of the pellets is used as pristine for comparison with an irradiated one. The pellets are irradiated with 100 MeV swift Si^{8+} ion beam with current 2 pnA for the fluence in the range 1×10^{11} to 1×10^{14} ion cm^{-2}, using a 15 UD Pelletron at Inter University Accelerator Center (IUAC), New Delhi, India [16]. The samples are mounted on glass side of 10 cm length, 2.5 cm width 2 mm thickness. Then the slide is carefully on a copper target ladder using double sided tape. The ion beam is magnetically scanned on a 1×1 cm area on samples surfaces for a uniform irradiation and spot sizes were 2.5 mm^2 [17]. Four pellets are exposed to the same amount of fluence at a time each one for XRD, FTIR, TL and PL studies. PL emission spectra are recorded using Perkin Elmer LS55 spectrometer in the range 350–700 nm. The Samples are excited using a Xenon lamp in the range 252 nm. All experiments are done at room temperature. TL glow curves are recorded using a Harshow TLD reader (Model 3500) fitted with a 931B PMT having a neutral density filter at the heating rate of 5 Ks^{-1} in the temperature range from 323 to 650 K. The irradiated surface is kept facing upwards towards the detector [photomultiplier tube (PMT)] of the TLD reader.

3. Results and discussion

Swift heavy ions (SHI) interacting with material loses its electronic energy and nuclear energy and cause intense electronic excitations along the ion trajectory that may result in defect clusters and/or ion tracks can be created along the range. The defect structure depends on the energy loss values and irradiated fluences or amorphization or phase transformation on nanometer scale. Thus, it is interesting to know the effect of strong electronic excitation by energetic heavy ions in the surface region of materials. For 100 MeV Silicon ions for yttrium oxide target in the present studies, Se and Sn are calculated using SRIM 2003 program to be 4.047 and 3.29×10^{-3} keV nm^{-1}, respectively [18]. Here, the Se is higher than the threshold required for the creation of extended defects, hence it suggested the creation of larger number of color centre and point defects in Si^{8+} ion irradiated Y_2O_3. S_e is dominant up to 22.26 μm from the surface (www.srim.org) [19].

Fig. 2(a) shows the PXRD patterns of as prepared and annealed yttria. The diffraction peaks are found to be in good agreement with the JCPDF No. 88-1040. The diffraction peaks become stronger

and sharper with the increase of annealing temperature, the powders was showed crystallized when annealed at the temperature of 600 °C and found to be cubic crystal system with the space group $1\alpha\ \bar{3}$ and possess main peaks at $2\theta = 20.53$, 29.16, 33.81, 39.89, 43.47, 48.53, 57.60, 60.48, 64.51 corresponding to (211), (222), (400), (332), (134), (440), (622), (444), (721) planes. No impurity peaks in the PXRD profile and it confirms the formation of single phase cubic crystalline yttrium oxide nanoparticals [6]. The average crystallite size of Y_2O_3 is estimated by Debye–Scherrer's equation (1).

$$D = \frac{0.9\lambda}{\beta \mathrm{Cos}\theta} \tag{1}$$

where, D is the crystallite size, λ is the wavelength of X-ray (1.5406 Å), β is the full width at half maxima (FWHM) calculated by using origin software and θ is the Bragg angle. The average crystallite sizes are found to be ~13.01 nm for sample annealed at 600 °C, whereas, 900 °C annealed sample shows ~30.85 nm XRD peaks at sample annealed at 900 °C indicates enhancement in crystallinity as compared to those sample annealed at 600 °C. Further inter-planar spacing (d), lattice constant (a), cell volume (V) density (p), dislocation density (δ) and effective strain (ε) are also calculated and given in Table 1. The effective strain and crystallite size can be measured by using Williamson–Hall (W–H) method following Eq. (2).

$$\frac{\beta \mathrm{Cos}\theta}{\lambda} = \frac{1}{D} + \frac{4\varepsilon \mathrm{Sin}\theta}{\lambda} \tag{2}$$

where, 'β' is the full width at half maxima (FWHM), 'λ' is the wavelength of X-ray (1.5406 Å), 'D' is the crystallite size, 'θ' is the Bragg angle and 'ε' is the effective strain. A plot of β Cos(θ/λ) and Sin(θ/λ) will yield a straight line with a slope equal to the value of the effective strain and y-intercept equal to the inverse of the crystallite size [20]. Fig. 2(b) shows the W–H plot for Y_2O_3 samples annealed at different temperature. The average crystallite size for which strain has been taken into it is found to be ~13.25 nm for sample annealed at 600 °C, whereas, 900 °C annealed samples show ~40.02 nm and

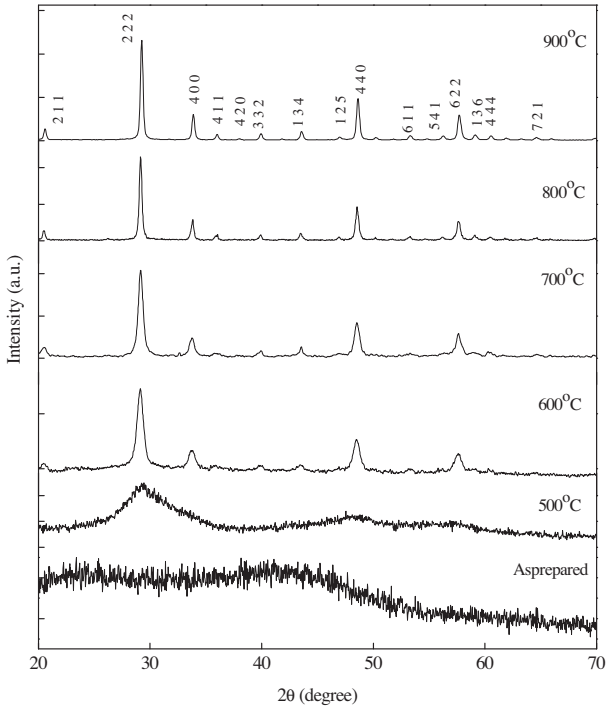

Fig. 2a. PXRD pattern of sol–gel synthesized Y_2O_3 at different temperature.

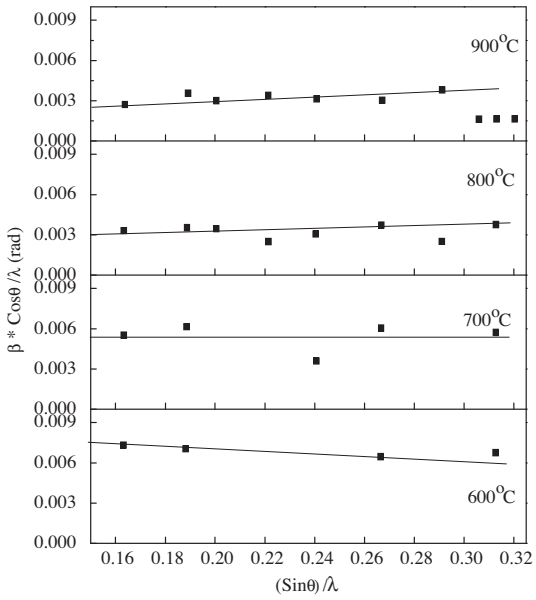

Fig. 2b. W–H plot for the sol–gel synthesized pure Y_2O_3 at different temperature for 2 h.

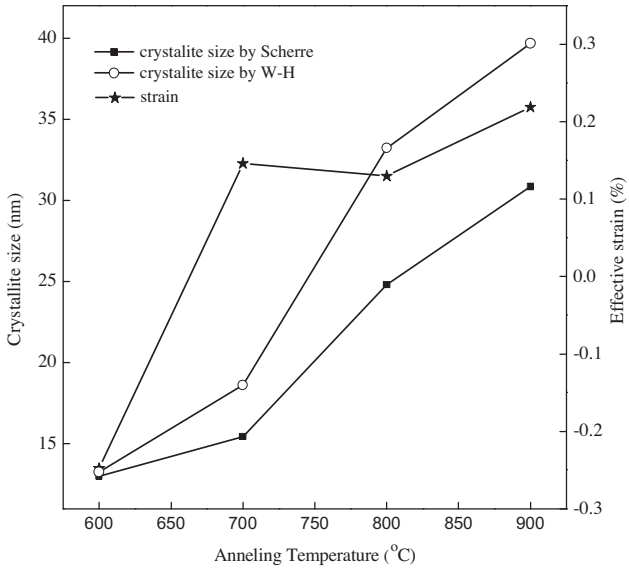

Fig. 2c. Variation of crystallite size and effective strain with annealing temperature.

strains has to be found as shown in Table 1. In both methods, the crystallite size linearly increase with increasing temperature but 600 °C heat treated sample shows the negative effective strain due to at 600 °C heat treated sample do not complete crystallite nature therefore it act as a compressive force and 700 °C and above heat treated sample shows positive effective strain due to tensile fore and effective strain slowly increases with increasing temperature as shown in Fig. 2(c).

The density (p), dislocation density (δ) and effective strain (ε) are calculated using the following relations (3)–(5) [21],

$$\rho = \frac{16M^3}{\mathrm{Na}} \tag{3}$$

$$\delta = \frac{1}{D^2} \tag{4}$$

Table 1
XRD structural parameters of heat treated Y_2O_3.

Temperature (°C)	Crystallite size D (nm)		Lattice constant a (Å)	Cell volume (Å^3)	Density ρ (g cm^{-3})	Dislocation density δ ($\times 10^{15}$)	Inter-planar space in at (222) (Å)	Effective strain (%)	
	Debye Scherer	W–H method						W–H method	Calculated
600	13.01	13.25	10.602	1195.079	5.034	5.696	3.0605	-0.248	0.282
700	15.45	18.61	10.610	1198.049	5.022	4.189	3.0631	0.146	0.212
800	24.79	33.22	10.613	1190.168	5.018	1.627	3.0638	0.130	0.127
900	30.85	40.02	10.618	1195.054	5.012	1.051	3.0651	0.105	0.124

$$\varepsilon = \frac{\beta \cos\theta}{4} \tag{5}$$

where M is the molecular mass, N is the Avogadro number, the density, dislocation density and effective strain calculated are tabulated in Table 1. It shows that the density of samples and dislocation density decreases with increasing the annealing temperature due to enhancement of crystallite size.

Further, the effect of SHI irradiation on crystallite size in 900 °C annealed pellets is studied. Fig. 3(a) shows the XRD patterns of pristine and SHI irradiated Y_2O_3. The average crystallite size for 100 MeV Si^{8+} ion irradiated for the fluence of 1×10^{14} ion cm^{-2} is found to be 23.84 nm. Thus the crystallite size is found to be decreased when irradiated with pristine [22]. W–H method is used to calculate the effective strain and the average crystallite size. From W–H plot, average crystallite size is found to ~40.02 nm for pristine and ~35.20 nm for SHI irradiated sample. Further, the effective strain decreases for SHI irradiated sample as shown the Fig. 3(b). Also, density, dislocation density and effective strain are calculated for ion irradiated samples and tabulated in Table 2. Moreover, the FWHM increases and the intensity of the peak decrease with irradiation. This implies that the effect of ion irradiation do not affect the structure of these sample.

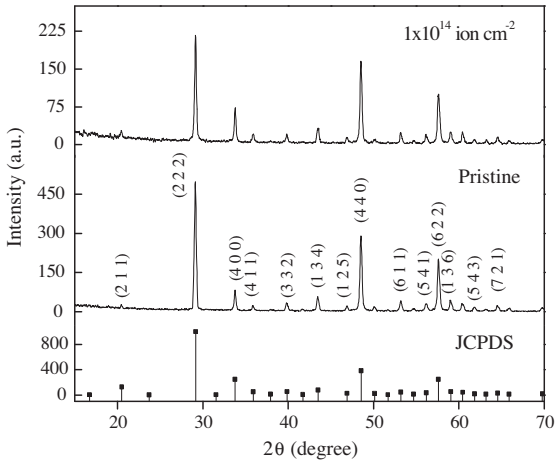

Fig. 3a. PXRD pattern of pristine and 100 MeV Si^{+8} ions irradiated Y_2O_3.

Fig. 4 shows the FTIR spectra of the dried gel and annealed for different temperatures. The strong vibration band at 3434 cm^{-1} indicates the presence of hydrogen bonds involved in O–H oscillators, arising from adsorbed moisture in the atmosphere. In solid citrate the carboxyl groups are ionized, so the peak at 1400 and 1525 cm^{-1} may be assigned to COO^- group vibration of the citrate complex, the shoulder at 1724 cm^{-1} might be corresponds to the COOR groups, caused by the dimer of free citric acid. The peak observed at 465 and 564 cm^{-1} are attributed to the stretching of Y–O bond. The peak at 847 cm^{-1} is due to the absorption of small amount of CO_3^{-2} [6]. As the annealing temperature increases, the absorption intensity of the COO^- group decreases due to the decomposition of the citrate complex and CO_3^{-2} peak intensity also decreases and finally disappears. The peaks at 465 and 564 cm^{-1} appears for 600 °C annealed sample, indicates that amorphous gel powder is converting to crystalline form. This result is correlated with PXRD result. Further increasing in annealing temperature increases the absorption peak intensity due to the increase in crystallinity of the sample.

Fig. 5 shows the FTIR spectrum of sol–gel synthesized 900 °C annealed SHI irradiated Y_2O_3. The absorption bands with peaks at 420, 465, 564, 671, 1060, 1426, 1543, 1650, 1748, 2338, 2360, 2925, 3450 and 3752 cm^{-1} are observed in pristine sample. Further, when the sample is irradiated with 100 MeV swift Si^{8+} ions with ion fluence 1×10^{14} ions cm^{-2}, the absorption band at 1060

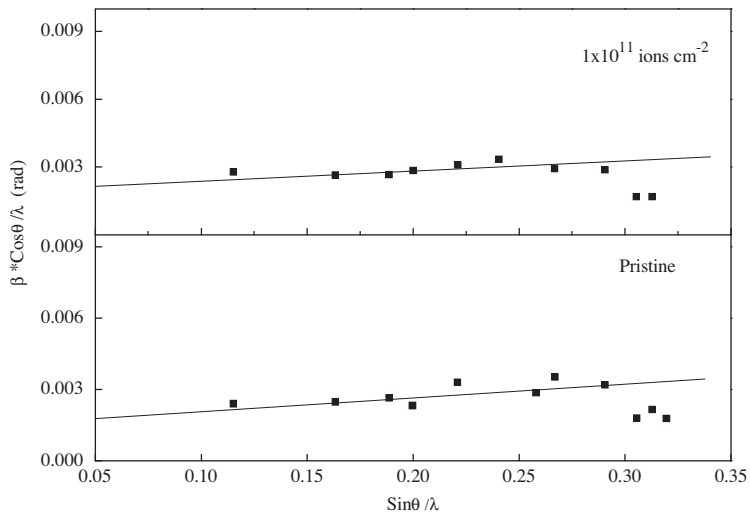

Fig. 3b. W–H plot for the sol–gel synthesized 900 °C heat treated Y_2O_3.

Table 2
XRD structural parameters of Pristine and 100 MeV swift Si^{8+} with ion fluence 1×10^{14} ions cm^{-2} irradiated Y_2O_3.

Temperature (°C)	Crystallite size D (nm)		Lattice constant a (Å)	Cell volume (Å^3)	Density ρ (g cm^{-3})	Dislocation density δ ($\times 10^{15}$)	Inter-planar space in at (222) (Å)	Effective strain (%)	
	Debye Scherer	W–H method						W–H method	Calculated
Pristine	30.85	40.02	10.618	1195.054	5.012	1.051	3.0651	0.105	0.124
1×10^{14}	23.84	35.20	10.588	1186.983	5.054	1.759	3.067	0.010	0.099

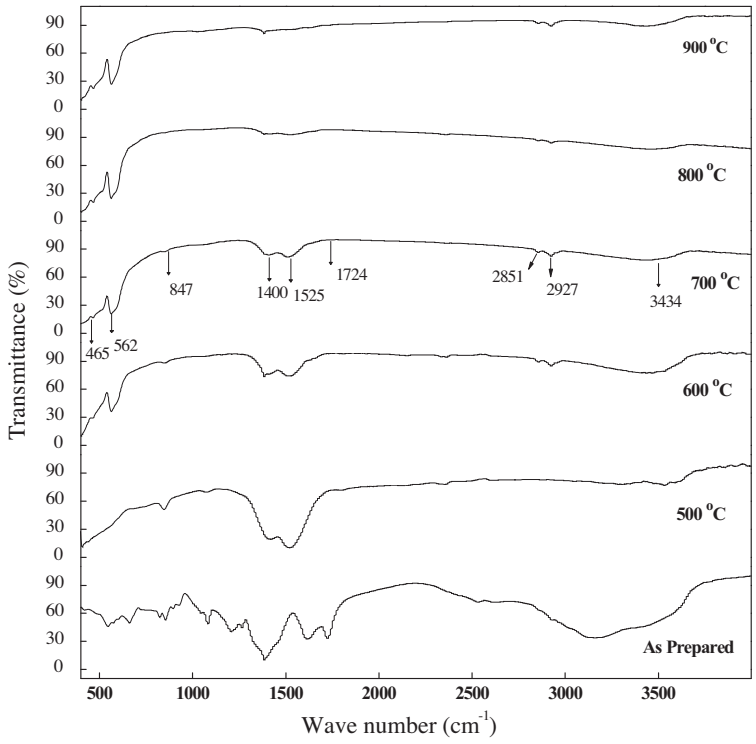

Fig. 4. FT-IR spectra of sol–gel synthesized Y_2O_3 at different temperature.

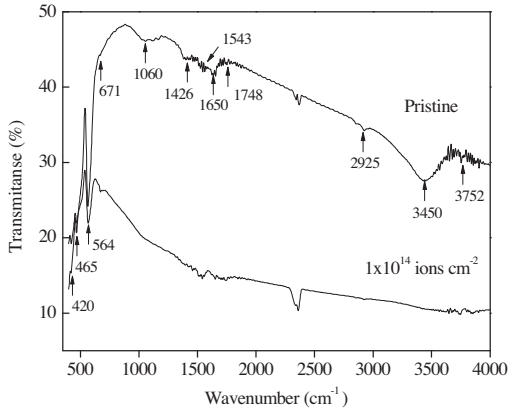

Fig. 5. FT-IR spectra of sol–gel synthesized 900 °C heat treated pristine and 100 MeV swift Si^{8+} ions irradiated Y_2O_3.

and 3450 $cm^{-1}$are disappeared and the results are tabulated in Table 3. The absorption in the region 1426–1650, 3450–3752, 420–566, 671, 1060, 1748 and 2925 cm^{-1} are attributed to COO^- vibration, O–H stretching, Y–O stretching, COOR and O–H stretching, respectively. The peaks at 420, 467 and 566 cm^{-1} are attributed to Y–O stretching [6,22,23]. When the sample is irradiated with 100 MeV Si^{8+} ions, a large amount of energy is deposited

Table 3
FTIR absorption peaks of pristine and 100 MeV swift Si^{8+} with ion fluence 1×10^{14} ions cm^{-2} irradiated Y_2O_3.

FTIR absorption peaks (cm^{-1})		
Pristine	Ion-irradiated with fluence 1×10^{14} (ion cm^{-2})	Modes
420	420	Y–O Stretching
467	465	Y–O Stretching
566	564	Y–O Stretching
671	671	COO^- Stretching
1060	–	COO^- Stretching
1426	1426	COO^- Stretching
1555	1543	COO^- Stretching
1635	1650	COO^- Stretching
1748	1748	COOR vibration
2925	2925	–OH
3450	–	–OH (γ_1, γ_2)
3752	3752	–OH Stretching

in the system through electronic energy loss. This energy to break the bonds corresponding to COO^- stretching and O–H stretching in Y_2O_3 [22].

3.1. Photoluminescence

Photoluminescence of yttrium oxide samples irradiated with 100 MeV Si^{8+} ions for fluences in the range 1×10^{11} to 1×10^{14}

Table 4
Trap parameters of TL glow of 100 MeV swift Si^{8+} with ion fluence 1×10^{11} ions cm^{-2} irradiated Y_2O_3.

Ion fluence (ions cm^{-2})	Peak	T_m (K)	μ_g	Order of kinetics	E_{av} (eV)	s (s^{-1})	n_o (cm^{-3})
1×10^{11}	Tm_1	430	0.51	1.6	0.954	4.650×10^{10}	3.203×10^6
	Tm_2	538	0.49	1.6	0.814	6.629×10^6	3.268×10^6
	Tm_3	584	0.49	1.6	1.754	4.330×10^{14}	5.609×10^6

ions cm^{-2} is shown in Fig. 6(a). The PL spectrum is recorded using 252 nm Xenon beam excitation. Sharp emission band with peaks at 417, 432 and 465 nm are observed in both pristine and SHI irradiated samples. Based on the studies an aluminum oxide the emission bands observed in the present work with peaks at 417, 432 and 465 nm are attributed to F, F^+ and F_2^+ centers respectively [22,24,25]. The intensity of these emission peaks varies with the ions fluence. The PL intensity increases with increase in ions fluence up to 3×10^{11} ions cm^{-2} then decreases with further increase of ions fluence as can be seen in Fig. 6(b). This might be due to the increase in concentration of primary defect center (F and F^+). This defect center start aggregating once their concentration become high and gives raise to pairs of oxygen vacancies (F_2-type center) [26]. The PL intensity decreases with higher fluence which may be attributed to annihilation of F^+ center resulting from a disorder and induced defect center clustering and also diffusion of defect centers [25]. SHI irradiation creates a latent track in a target material when Se exceeds a threshold value (Se_{th}). With higher fluence for primary defect centers (F centre) convert into F^+ or F_2^+ defect centers. In previous studies it is reported that swift Ag^{8+} ion irradiated mullite samples show increase in PL intensity up to 5×10^{11} ions cm^{-2} and is attributed to creation of additional defect centers responsible for PL during the bombardment process. The decrease in PL intensity with further increase of ion fluence implies some changes in the energy levels of the crystal resulting from the perturbation of the luminescent sites and from transient defect states formed during the bombardment process. The sample in this case is supposed to be amorphized as a result of cascade quenching with swift heavy ion irradiation [27].

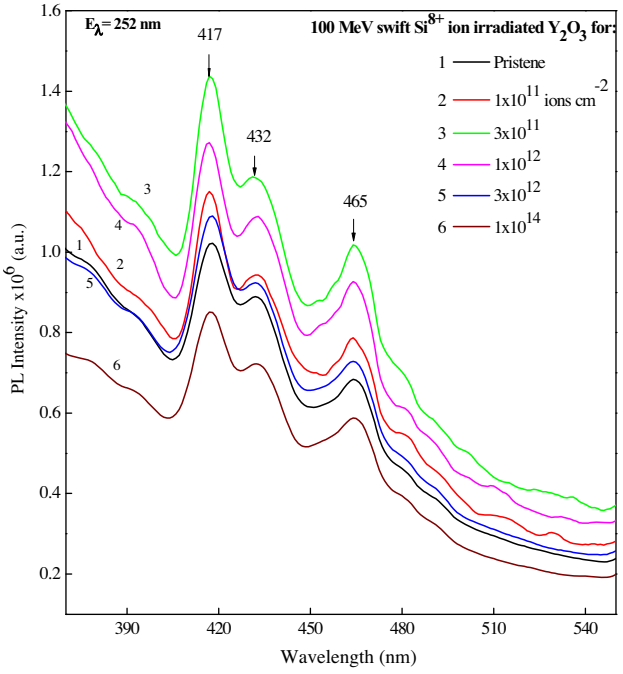

Fig. 6a. PL emission (E_λ = 252 nm) spectra of sol–gel synthesized 900 °C heat treated 100 MeV swift Si^{8+} ion irradiated Y_2O_3.

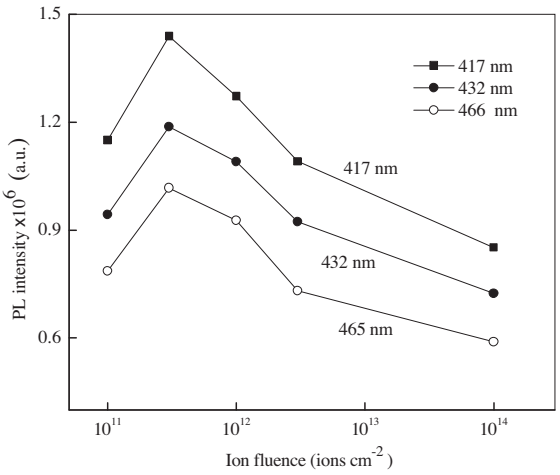

Fig. 6b. Variation in PL intensity with 100 MeV swift Si^{8+} ion fluence in Y_2O_3.

3.2. Thermoluminescence

Thermoluminescence is a very common and simple technique used for estimation of doses of high energy ionizing radiations absorbed in materials. As-synthesized heat treated Y_2O_3 pellets do not show any thermoluminescence response. However, thermoluminescence glow curves obtained due to 100 MeV Si^{8+} ion irradiation for fluences in the range 1×10^{11} to 1×10^{14} ions cm^{-2} at room temperature one shown in Fig. 7(a). One TL glow a well-resolved glow with peak at ~430 K (Tm_1) and two unresolved glows with peak at ~540 K (Tm_2) and ~580 K (Tm_3) are observed [26]. Two TL glow with peaks around 475 and 626 K in γ-irradiated Y_2O_3 were reported from the same laboratory when disodium ethylene diamine tetre acetic acid (EDTA-Na_2) was used as fuel in the combustion process [6]. In present work Fig. 7(b) shows the variation in TL glow peak intensity (Im_1 and Im_2) with fluence in 100 MeV Si^{8+} ion irradiated nanocrystalline yttrium oxide. It is found that, the glow peak intensity at Tm_1 decreases continuously with increasing ion fluence. And that at Tm_2 is increase with increasing ion fluence up to 1×10^{12} ions cm^{-2} and then decreases with increasing ion fluence as can be seen from Fig. 7(b). This may be correlated with the observed above PL results.

The evaluation of kinetic parameters (trapping parameters), i.e. activation energy (E) of the traps involved in TL emission, order of kinetics (b), frequency factor (s) and trap density (n_o) associated with the glow peaks of TL, is one of the important aspects of studies in condensed matter physics. Any complete description of the TL characteristics of material requires the complete knowledge of these parameters. Here, E is the energy required for the release of charge carrier from the trap to reach its excited state and 's' is the rate of electron ejection. The order of kinetics b is a measure of the probability that a free electron gets retrapped. This retrapping effect also depends on the availability of empty traps. The retrapping effect increases with the density of empty traps. To obtain these parameters, the glow curves are deconvoluted using Origin 7.5 software. The trap parameters of deconvoluted curves

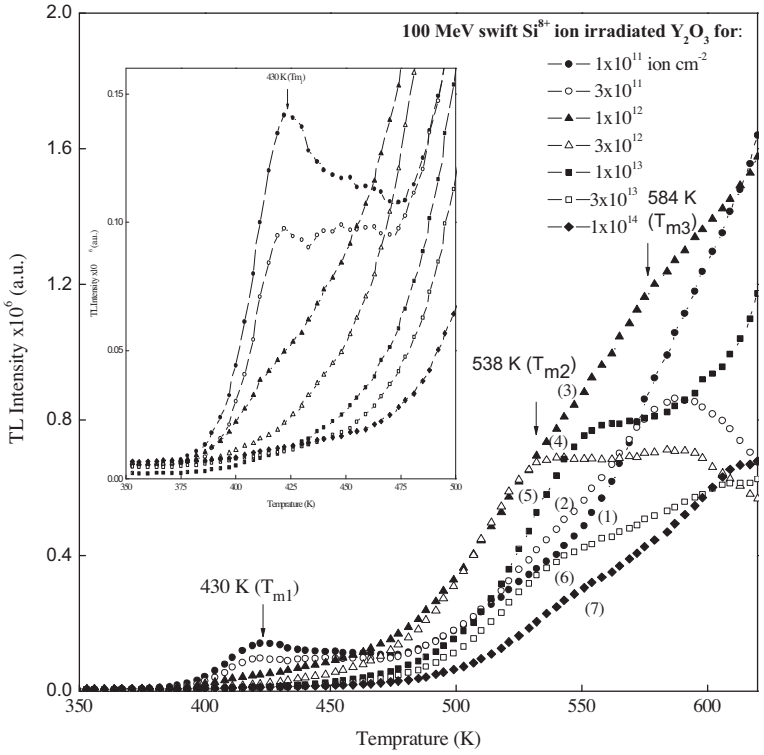

Fig. 7a. Thermoluminescence glow curves 900 °C heat treated 100 MeV swift Si^{8+} ion irradiate Y_2O_3.

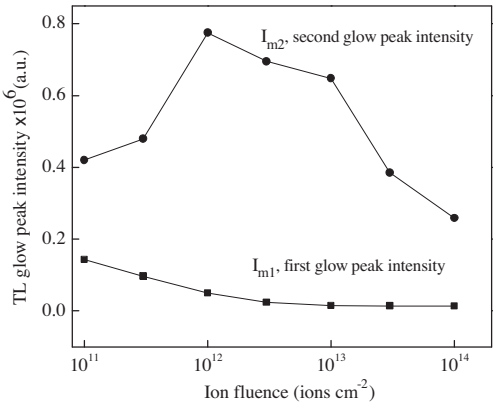

Fig. 7b. Variation of TL glow peak (Im_1 and Im_2) intensity with fluence.

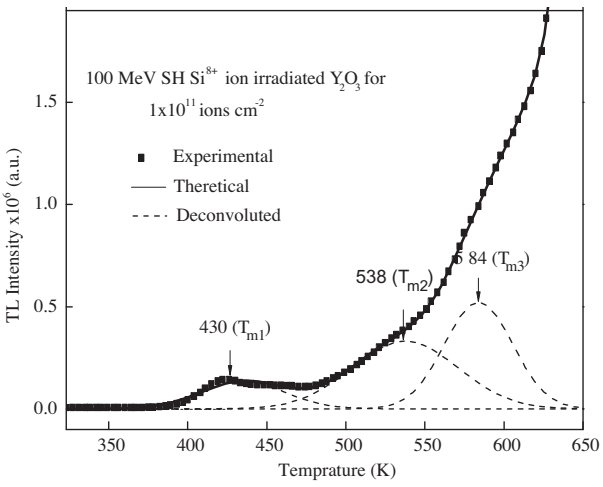

Fig. 7c. Deconvoluted thermoluminescence glow curve of SHI irradiated Y_2O_3 (1×10^{11} ions cm^{-2}).

are calculated using the glow curve shape method [28]. Trap density (n_o) is calculated using the relation (6) [29].

$$n_o = \frac{\omega I_m}{\beta\{2.52 + 10.2(\mu_g - 0.42)\}} \tag{6}$$

where $\omega = T_2 - T_1$, β is the heating rate and μ_g is symmetry factor.

Fig. 7(c) shows the deconvoluted glow curve of nanocrystalline yttrium oxide irradiated for the fluence of 1×10^{11}–1×10^{14} - ions cm^{-2}. The deconvolution of the experimental curves revealed TL glow peaks at 430, 538 and 584 K. One can define a geometry factor μ_g typically closed 0.42 for first-order glow peak and 0.52 for second order glow peak. In the present work μ_g is calculated to be 0.51, 0.49 and 0.49 (see Table 4) this implies that glow curve indicates the second order kinetics. The reason for this a large band gap in the nanophosphor shows a higher probability of charges getting retrapped during TL emission.

4. Conclusions

Nanocrystalline yttrium oxide is synthesized by sol–gel technique using citric acid ($C_6H_8O_7$) as chelating agent at low temperature. The XRD result showed that the Y_2O_3 powders completely crystallized at 600 °C. The crystallites sizes are found to increase with increasing annealing temperature and ion irradiated XRD showed that crystallite size is decreased. FTIR results of as synthesized and ion irradiated Y_2O_3 indicates the formation for Y_2O_3 and the destruction of COO^- and –OH stretching. PL of 100 MeV Si^{8+} ion irradiated samples shows emission with peaks at 417, 432 and 465 nm due to F, F^+, F_2^+ defect centers. It is found that PL intensity increases with increasing in ion fluence up to $\sim 3 \times 10^{11}$ ions cm^{-2} and decreases with further increase in ion fluence due to creation

of new defects. The low temperature TL glow peak intensity at Tm_1 (~430 K) decreases continuously while that another glow peak intensity Tm_2 (~540 K) increase initially and decreases with increasing ion fluence. The deconvolution of the experimental TL curves revealed TL glows with peaks at 430, 538 and 584 K which overlap in the actual experimental TL glow curve.

Acknowledgements

The authors express their sincere thanks to Dr. D.K. Avasthi, Materials Science Division, Dr. S.P. Lochab, Health Physics Division, Inter University Accelerator Centre (IUAC), New Delhi, India for their constant encouragement and help during the experiment. Also, one of the authors (N.J.S.) is grateful to IUAC, New Delhi, for providing fellowship under UFR (No. 48303) scheme.

References

[1] Lin Wang, Yuexiao Pan, Yang Ding, Wenge Yang, Wendy L. Mao, Stanislav V. Sinogeikin, Yue Meng, Guoyin Shen, Ho-kwang Mao, Appl. Phys. Lett. 94 (2009) 061921.
[2] Akihiro Fukabori, Masami Sekita, Takayasu Ikegami, Nobuo Iyi, Toshiki Komatsu, J. Appl. Phys. 101 (2007) 043112.
[3] B.H. O'Connor, T.M. Velentine, Acta Crystallogr. B 25 (1969) 2140.
[4] M. Faucher, J. Pannetier, Acta Crystallogr. B 36 (1980) 3209.
[5] Hui Huang, Xuhui Sun, Suidong Wang, Yang Liu, Xiaorui Li, Jinglin Liu, Zhenhui Kang, Shuit-Tong Lee, Dalton Trans. 40 (2011) 11362.
[6] B.N. Lakshminarasappa, J.R. Jayaramaiah, B.M. Nagabhushana, Powder Technol. 217 (2012) 7.
[7] T. Mimani, K.C. Patil, Mater. Phys. Mech. 4 (2001) 134.
[8] J. Lee, Y. Tak, J. Ind. Eng. Chem. (1999) 5139.
[9] Rajesh Kumar, S. Asad Ali, A.K. Mahur, H.S. Virk, F. Singh, S.A. Khan, D.K. Avasthi, Rajendra Prasad, Nucl. Instr. Meth. Phys. Res., B 266 (2008) 1788.
[10] S.W.S. Mckeever, Thermoluminescence of Solids, Cambridge University Press (1985).
[11] A.J.J. Bos, Nucl. Instr. Meth. B 184 (2001) 3.
[12] M.S. Zhang, Z. Yin, Phys. Status Solidi 179 (2000) 319.
[13] A. Dupont, C. Parent, B. Le Garrec, J.M. Heintz, J. Solid State Chem. 171 (2003) 152.
[14] Chen Weifan, Li Fengsheng, Liu Leili, Yongxiu, J. Rare Earths 24 (2006) 543.
[15] Shibani Das, Study of composition behavior of binders and the effect of bender type on strength and density of Alumina samples (B.Tec thesis), 2011.
[16] D. Kanjilal, S. Chopra, M.M. Narayanan, S. Iyer Indira, R.J.J. Vandana, S.K. Datta, Nucl. Instr. Meth. Phys. Res., A 328 (1993) 97.
[17] Numan Salah, S.P. Lochab, D. Kanjilal, Ranju Ranjan, Sami S. Habib, J. Appl. Phys. 102 (2007) 064904.
[18] J.F. Ziegler, J.P. Biersack, M.D. Ziegler, SRIM – The Stopping and Range of Ions in Matter, Lulu Press Co, USA, 2008.
[19] Song Yin, Xie Er-qing, Zhang Chong-hong, Wang Zhi-guang, Zhou Li-hong, Ma Yi-Zhong, Yao Cun-feng, Zang Hang, Liu Chun-bao, Sheng Yan-bin, Gou Jie, Nucl. Instr. Meth. Phys. Res., B 266 (2008) 2998.
[20] Rene Guinebretière, X-ray Diffraction by Polycrystalline Materials, First published in France in 2002 and 2006 by Hermes Science.
[21] A. Vij, R. Kumar, A.K. Chawla, S.P. Lochab, R. Chandra, N. Singh, Opt. Mater. 33 (2010) 58.
[22] K.R. Nagabhushana, B.N. Lakshminarasappa, G.T. Chadrappa, D. Haranath, Fouran Singh, Rad. Eff. Def. Solids 162 (2007) 325.
[23] Bui Van Hao, Pham Thanh Huy, Tran Ngoc Khiem, Nguyen Thi Thanh Ngan, Pham Hong Duong, J. Conf. Series 187 (2009) 012074.
[24] K.S. Jheeta, D.C. Jain, Ravi Kumar, K.B. Garg, Solid State Commun. 144 (2007) 460.
[25] K.S. Jheeta, D.C. Jain, Ravi Kumar, Fouran Singh, K.B. Garg, J. Nucl. Mater. 353 (2006) 190.
[26] R.J. Gaboriaud, F. Paumier, M. Jublot, B. Lacroix, Nucl. Instr. Meth. Phys. Res., B 311 (2013) 86.
[27] H. Nagabhushana, B.N. Lakshminarasappa, S.C. Prashantha, K.R. Nagabhushana, Fouran Singh, Nucl. Instr. Meth. Phys. Res., B 244 (2006) 31.
[28] K.R. Nagabhushana, B.N. Lakshminarasappa, Fouran Singh, Radiat. Meas. 43 (2008) S651.
[29] N. Suriyamurthy, B.S. Panigrahi, J. Lumin. 128 (2008) 1809.